The Planetary Fourier Spectrometer (PFS) for Mars Express

V. Formisano[1], D. Grassi[1], R. Orfei[1], D. Biondi[1], E. Mencarelli[1], A. Mattana[1], F. Nespoli[1], A. Maturilli[1], M. Giuranna[1], M. Rossi[1], M. Maggi[1], P. Baldetti[1], G. Chionchio[1], B. Saggin[2], F. Angrilli[2], G. Bianchini[2], G. Piccioni[3], A. Di Lellis[3], P. Cerroni[3], F. Capaccioni[3], M.T. Capria[3], A. Coradini[3], S. Fonti[4], V. Orofino[4], A. Blanco[4], L. Colangeli[5], E. Palomba[5], F. Esposito[5], D. Patsaev[6], V. Moroz[6], L. Zasova[6], N. Ignatiev[6], I. Khatuntsev[6], B. Moshkin[6], A. Ekonomov[6], A. Grigoriev[6], V. Nechaev[6], A. Kiselev[6], Y. Nikolsky[6], V. Gnedykh[6], D. Titov[6], P. Orleanski[7], M. Rataj[7], M. Malgoska[7], A. Jurewicz[7], M.I. Blecka[7], H. Hirsh[8], G. Arnold[8], E. Lellouch[9], A. Marten[9], T. Encrenaz[9], J. Lopez Moreno[10], S. Atreya[11] & P. Gobbi[12]

[1]*Istituto di Fisica dello Spazio Interplanetario CNR (IFSI), Via del Fosso del Cavaliere 100, I-00133 Roma, Italy*
Email: formisan@nike.ifsi.rm.cnr.it
[2]*Universita di Padova, Dipartimento Ingegneria Meccanica (DIUNP), Via Venezia 1, I-35131 Padova, Italy*
[3]*Istituto Astrofisica Spaziale CNR (IAS), Reparto di Planetologia, Viale dell'Universita 11, I-00185 Roma, Italy*
[4]*Universita degli Studi di Lecce, Dipartimento di Fisica Via Arnesano, I-73100 Lecce, Italy*
[5]*Osservatorio Astronomico di Capodimonte (OAC), Via Moiariello 16, I-80131 Napoli, Italy*
[6]*Space Research Institute of Russian Academy of Sciences (IKI), Profsojuznaja 84/32, 117810 Moscow, Russia*
[7]*Space Research Center of Polish Academy of Sciences (SRC PAS), Bartycka 18A, 00716 Warsaw, Poland*
[8]*Deutsche Forschungsansalt fur Luft und Raumfahrt (DLR), Institut fur Planetenerforschung, Rudower Chausse 5, D-12489 Berlin Adlershoft, Germany*
[9]*Observatoire de Paris Meudon, Department de Recherch Spatiale (DESPA), Place J. Janssen 5, F-922195 Meudon, France*
[10]*Istituto de Astrofisica de Andalusia CSIC, p.o.b. 3004, E-18080 Granada, Spain*
[11]*The University of Michigan, Planetary Science Laboratory, 2455 Hayward Ave., Ann Arbor, MI 48109-2143, USA*
[12]*Istituto di Fisica dell'Atmosfera CNR (IFA), Via del Fosso del Cavaliere 100, I-00133 Roma, Italy*

The Planetary Fourier Spectrometer (PFS) for the Mars Express mission is optimised for atmospheric studies, covering the IR range of 1.2-45 μm in two channels. The apodised spectral resolution is 2 cm^{-1}, while the sampling is 1 cm^{-1}. The FOV is about 2º for the short wavelength (SW) channel and 4º for the long wavelength (LW) channel, corresponding to spatial resolutions of 10 km and 20 km, respectively, from an altitude of 300 km. PFS will also provide unique data on the surface-atmosphere interaction and the mineralogical composition of the surface. It will be the first Fourier spectrometer covering 1-5 μm to orbit the Earth or Mars.

The experiment has real-time onboard Fast Fourier Transform (FFT) in order to select the spectral range of interest for data transmission to ground. Measurement of the 15-μm CO_2 band is very important. Its profile gives, via a complex temperature-profile retrieval technique, the vertical pressure temperature relation, which is the basis of the global atmospheric study. The SW channel uses a PbSe detector cooled to 200-220K, while the LW channel is based on a pyroelectric ($LiTaO_3$) device working at room temperature. The interferogram is measured at every 150 nm displacement step of the corner cube retroreflectors (corresponding to 600 nm optical path difference) via a laser

diode monochromatic interferogram (a sine wave), with the zero crossings controlling the double pendulum motion.

PFS will operate for about 1.5 h around the pericentre of the orbit. With a measurement every 10 s, 600 measurements per orbit will be acquired, corresponding to 224 Mbit. Onboard compression will reduce it to 125 Mbit or less, depending on the allocated data volume per day. An important requirement is to observe at all local times in order to include night-side vertical temperature profiles. Total instrument mass is 31.2 kg.

1. Scientific Objectives

1.1 Introduction

In the past 30 years, ground-based observations and space missions have built an impressive body of information about Mars. Nevertheless, a large number of questions remain open. One of the most interesting problems is the evolution of the climate and atmosphere in relation to water. It is widely believed that the younger Mars possessed a dense atmosphere and liquid water on the surface. However, careful investigation of the recent atmosphere and surface is required for clarification.

The widespread use of IR spectroscopy in recent years for systematically studying planetary surfaces and atmospheres has detected molecular species in both major and minor quantities. Strong vibration-rotation bands in the 1-20 µm wavelength range are the fingerprints for unambiguous identification of chemical species. Many spectral bands of CO_2, H_2O and CO come within the range of sensitivity of PFS. Their detection will help to solve a wide set of scientific problems concerning atmospheric composition, solid-phase surface components and atmospheric dust.

In the near-IR range, where the incident solar radiation is either absorbed or scattered by molecules and dust grains, molecular bands usually appear in absorption. In the far-IR, molecular bands appear in both emission and absorption because the observed flux strongly depends on the thermal profile of the atmosphere.

However, even when the absolute intensities of the molecular bands are known from laboratory studies, it can be far from simple to derive the abundance of atmospheric constituents from a planetary spectrum. In the near-IR, a rough estimate of the absorber abundance can be obtained using the 'reflecting layer model'. This model assumes no scattering above a purely reflecting layer (cloud or surface). It is reasonable to apply it to the case of a tenuous atmosphere, such as that on Mars. Various methods can be used to determine the temperature-pressure T(P) relationship. In the cases of Mars, Venus and Jupiter, thermal profiles have been derived from strong absorption bands in the thermal-IR and also from radio occultation measurements by probes such as Mariner and Pioneer (Kliore et al., 1972; 1976). *In situ* measurements have been made on Mars and Venus.

Near-IR spectroscopy has greatly increased our knowledge of the surface composition and structure of planetary bodies, moons and asteroids. For planets with atmospheres, the identification of surface spectral signatures is strongly related to the simultaneous knowledge of the atmospheric structure. Electronic and molecular transitions occur at definite energies associated with near-IR wavelengths and result in the absorption of incident solar radiation by surface materials. In the visible and near-IR range (up to approximately 2.5 µm), transition of d-shell electrons and electron exchange between ions dominate. Particularly evident are the signatures from iron ions (e.g. McCord & Cruikshank, 1981). At longer wavelengths, the crystal structure and the nature of different rocks and minerals can be discriminated on the basis of the strength and position of absorption bands (e.g. Bartholomew et al., 1990).

A number of mineralogically significant bands of silicates, carbonates, sulphates, nitrates, phosphates, oxides and hydroxile-bearing materials occur in the thermal-IR. A great amount of laboratory work has been devoted to the systematic study of the relative strengths and positions of diagnostic spectral signatures (e.g. Hunt et al., 1974). Experimental results are supported by theoretical models in which the relations

Table 1. PFS scientific objectives.

Atmospheric studies: global long-term monitoring of the 3-D temperature field in the lower atmosphere (from the surface up to 40-60 km); measuring the variations of minor constituents (water vapour and carbon monoxide); searching for other minor components of the atmosphere; a new determination of the D/H ratio; studying the optical properties of atmospheric aerosols (dust clouds, ice clouds, hazes) and determining their size distributions and chemical compositions; investigating the radiance balance of the atmosphere and the influence of aerosols on atmospheric energetics; studying global circulation, mesoscale dynamics and wave phoenomena.

Surface studies: monitoring the surface temperature; determining the thermal inertia obtained from the daily surface temperature variations; determining the restrictions on the mineralogical composition of the surface layer; determining the nature of the surface condensate and seasonal variations of its composition; measuring the scattering phase function for selected surface locations; determining local pressure and height (CO_2 altimetry) for selected regions; surface-atmosphere exchange processes.

between IR spectral signatures and ion mass band strength and crystal structure were investigated (e.g. Carr, 1974).

1.2 The atmosphere of Mars

Mars resembles the Earth much more than any other planet in the Solar System, and studying its atmosphere provides a better understanding of our own. There is evidence of an earlier denser martian atmosphere, warmer climate and free water on the surface. However, explaining how warming was supported on the young Mars is not easy. The history of water on Mars is one of the most interesting problems in Solar System studies, and it directly connects with the possible presence of life on ancient Mars.

The investigations of Mars' atmosphere have determined an average composition of mainly carbon dioxide (95%), nitrogen (2.7%) and argon (1.6%) (Owen, 1992). About ten minor constituents have been identified. Of them, water vapour plays an important role in atmospheric processes and surface/atmosphere interactions. Water vapour bands will be observed by both PFS channels; monitoring water vapour variations (time, latitude, location) is an important task for PFS, and simultaneous observations in the two channels will provide estimates of H_2O vertical distribution.

The global annual average surface temperature of Mars is 210K (Arnold et al., 1993); the atmosphere is colder than Earth's at all heights. In general, the vertical structure of both can be divided into three main regions: low, middle (mesosphere) and upper (thermosphere). The middle atmosphere of Mars is its coldest region. Here is the sink for the energy flux coming from the surface and troposphere (heated by solar visible and near-IR) and the thermosphere. There are several important qualitative differences with the terrestrial atmosphere:

— there is no temperature maximum in the mesosphere;
— the lapse rate in the low atmosphere is less than on Earth;
— there are strong daily variations near the surface because of the much lower thermal capacity;
— the strong influence of aerosols on atmospheric heating.

The computation of realistic General Circulation Models (GCMs) is a very difficult task because it has to accommodate so many different effects. Horizontal differences in temperatures lead to differences in pressure, but they are smoothed by winds. Winds transfer heat together with air masses, influencing local temperature profiles. Temperatures are also affected by dust being lifted from the surface. Condensation is another route to aerosol formation, and it also feeds back to

temperatures. Winds vary with topography. However, a few groups of theoreticians have made significant large progress in GCM modelling. They work mainly with data from Mariner-9/IRIS for Ls 290-350° and much less for Ls 45-55° (full profiles; Ls is the angle between the Sun-Mars line and the northern spring equinox) and the much less informative Viking/IRTM atmospheric temperatures. PFS LW observations of the 15 µm band will help to fill the gaps. Such measurements will strengthen the empirical base for checking the martian GCMs.

Aerosols play a major role in the formation and variations of 3-D temperature and wind patterns in the atmosphere. There are two aerosol types: dust lifted from the surface, and condensates. A Global Dust Storm is the most pronounced manifestation of the influence of dust on martian meteorology, but aerosols are always present in the atmosphere and both kinds participate in heating/cooling processes. The chemical nature (minerals/ices), size distribution and optical depth of the aerosol medium will be estimated from PFS observations. Simultaneous observations by the two channels should be very helpful.

Previous data exhibited both seasonal and daily variations, and occasional climatic events. During northern winter, two different regimes have been observed in different years. In the first case, one or more dust storms cover nearly all the planet; in the second, there is no global storm but high winds raise dust in confined regions. By contrast, summer weather appears to be more repetitive: winds are generally low and evolve on a diurnal timescale. Storms are very peculiar events and require more detailed investigation. Pressure profiles, wind patterns and atmospheric dust-evolution must be carefully analysed to determine the effects on surface morphology. Surface changes produced by atmospheric activity have been revealed by observations of albedo patterns, and suggest close coupling of surface morphology with ambient evolution. In particular, chemical and physical processes at the lithosphere-atmosphere boundary must be better described and understood.

Temperature changes control the polar cap condensation rate and influence the formation and the evolution of clouds. Until now, white condensation (mainly water-ice) clouds have been observed; however, their evolution and detailed composition are still uncertain.

Atmospheric data can also be helpful, in combination with surface composition analyses, in determining the:

— distribution, abundance and physical status of water on the planet;
— volatile distribution and abundance in the atmosphere, on the crust, and at depth;
— outgassing processes.

The spectrum of Mars (as for any planet) consist of two elements: short wavelengths dominated by bireflected solar radiation, and long wavelengths dominated by the planet's thermal radiation. For Mars, the boundary between these two regimes is near 4 µm. The PFS SW and LW ranges almost match these regimes of the martian spectrum. Bands of atmospheric gases in the SW range appear only as absorption features; in the LW they can appear as absorption (if atmospheric temperature falls with height) or emission (if it rises), and occasionally the band may have a complicate shape.

1.3 Thermal sounding of the martian atmosphere

1.3.1 Physical background

In a strong absorption band, the thermal radiation emitted from the surface and lower atmospheric levels is absorbed by the higher regions and cannot escape to space. However, the strength of absorption bands usually varies by several orders of magnitude within a given spectral interval. If the outgoing radiation is measured across the entire band then different parts will bear information about the temperature at different altitudes.

The thermal sounding needs several conditions to be satisfied. First, the gas must

have spectral bands in the thermal-IR region. Second, the gas must be abundant enough to give strong absorption in the centre of the band in order to maximise the altitude range of sounding. Third, it is desirable that the gas is uniformly mixed within the bulk of the atmosphere and its abundance must not vary significantly with space, local time or season. Carbon dioxide meets these requirements rather well for the terrestrial planets. That is why CO_2 fundamental bands are usually chosen for thermally sounding the atmospheres of Venus, Earth and Mars.

The solution of radiative transfer equation for the outgoing radiation takes the form:

$$I(\nu) = \varepsilon(\nu)\, B(\nu, T_S)\, t\,(\eta_S, -\infty\,) + \int_{\eta_s}^{-\infty} B\,[\nu, T(\eta)]\, K(\nu, \eta)\, d\eta \qquad (1)$$

where ν is the wavenumber, η = log (*p*) (*p* is pressure) is the vertical coordinate, ε and T_S are the emissivity and temperature of the surface, respectively, *B* is the Planck function describing the blackbody radiation, *T*(η) is the vertical temperature profile, and

$$K(\nu, \eta) = -\frac{\partial t\,(\eta, -\infty\,)}{\partial \eta} \qquad (2)$$

is the weighting function, where $t\,(\eta, -\infty)$ is the transmittance between the atmospheric level η and space along the line-of-sight. The first term in Eq. (1) corresponds to the radiation from the surface attenuated by the atmosphere. The second one describes the emission of the atmosphere. The weighting functions *K* (ν, η) define the weight with which the atmospheric layer at pressure η contributes to the radiation measured at wavenumber ν. Eq. (1) is written under the following assumptions:

— the atmosphere is plane parallel. This is valid until the emission angle is smaller than ~80°;
— the scattering is neglected. This assumption is valid for almost all seasons on Mars because the dust loading is small. Only during dust storms should the scattering by dust be taken into account and Eq. (1) modified;
— it is assumed that the local thermodynamic equilibrium (LTE) requirement is met. This assumption means that the scattering in spectral lines is negligible and the energy of each absorbed photon is converted to the thermal energy of the gas via molecular collisions. This provides the necessary coupling between the radiation and kinetic temperature of the emitting gas. Detailed studies showed that the LTE conditions are fulfilled in the martian atmosphere at least in the altitude region 0-60 km, which will be covered by PFS.

1.3.2 PFS temperature sounding capabilities

The positions of the absorption bands of CO_2 gas in the PFS spectral region are shown in Fig. 1. The central wavenumbers and line intensities were taken from the HITRAN database (Rothman et al., 1992). Two very strong fundamental bands of CO_2 are in the thermal-IR region (200-2500 cm^{-1}) and they can be used for thermal sounding. The first at 15 μm is in the region of maximum radiation from Mars and is optimal for thermal sounding. The band at 4.3 μm falls in the spectral interval where the thermal radiation is already low and the contribution from reflected solar light is not negligible. However, this band can be used at least at the night side to improve the quality of thermal sounding provided by the 15 μm band. PFS will be the first instrument to measure the outgoing radiation in these two bands simultaneously.

The altitude coverage and vertical resolution of the remote sensing are defined by

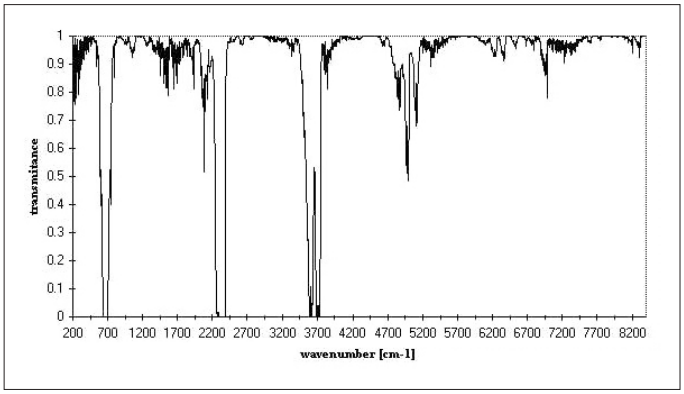

Fig. 1. Transmittance of gases in the atmosphere of Mars.

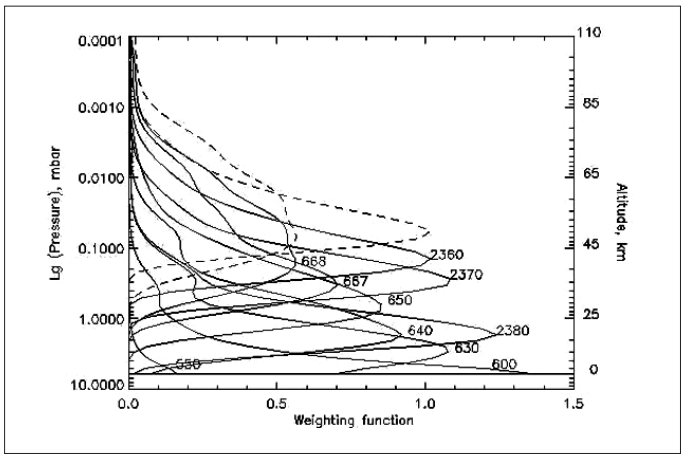

Fig. 2. Carbon dioxide weighting functions for the 4.3 μm and 15 μm absorption bands.

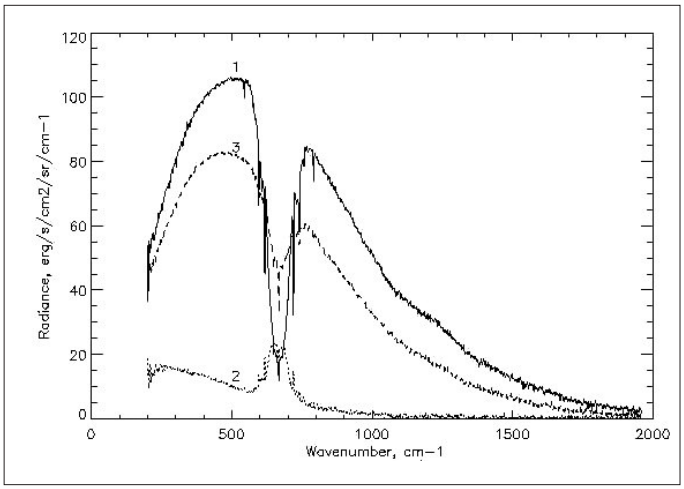

Fig. 3. Synthetic spectra in the LW channel of PFS.

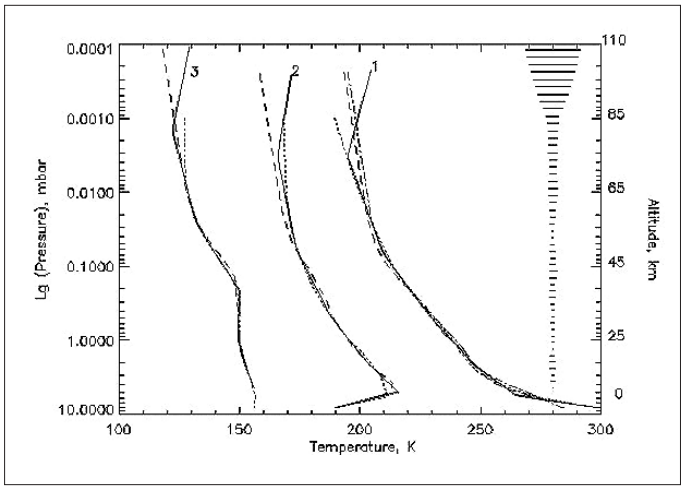

Fig. 4. Test temperature retrievals from PFS spectra.

the behaviour of weighting functions (Eq. 2). Examples of the weighting functions for PFS are shown in Fig. 2. The numbers on the curves designate the wavenumber: 550-668 cm^{-1} corresponds to 15 μm and 2360-2380 cm^{-1} to 4.3 μm. PFS weighting functions cover the pressure range from the surface up to ~10^{-3} mbar, corresponding to altitudes 0-70 km. However, the effectiveness of thermal sounding drops as the weighting functions decrease with altitude. The width of weighting functions is defined by the scale height of the atmosphere (~10 km) and the band structure. From Eq. 1 it is clear that broad weighting functions smooth small-scale features of the temperature profile. Nevertheless, practise shows that the features much smaller than the width of the weighting function can be retrieved from the emission spectrum because many spectral channels are used. The vertical resolution is estimated to be 3-5 km.

Additional use of the measurements in the 4.3 μm CO_2 band can improve the quality of the sounding, especially above 30 km. At these altitudes, the weighting functions for 15 μm (667 cm^{-1} and 668 cm^{-1}) are very broad. Those for the 4.3 μm band (2360 cm^{-1} and 2370 cm^{-1}) have smaller widths. These channels can provide better determination of the temperature profile above 30 km. The sounded region can

be extended upward by ~10 km in the off-nadir observations allowed by the PFS scanning capability. Fig. 2 (dashed lines) shows examples of weighting functions for slant geometry with emission angle of 80° for the 668 cm^{-1} and 2360 cm^{-1} channels.

1.3.3 Test temperature retrievals from PFS radiance spectra

The vertical temperature profile $T(\eta)$ is the solution of the non-linear integral Eq. 1 using the radiance measurements $I(\nu)$ in the CO_2 band. The solutions of this problem are unstable with respect to small perturbations of the right hand side of the equation. The experimental errors in the measured radiance spectrum can result in a non-physical temperature profile. The procedures that can provide a stable solution of the ill-posed problems are *regularisation* algorithms. They use various kinds of *a priori* information about the solution in order to select physically meaningful functions among mathematically possible solutions.

Several methods were developed to solve the thermal-sounding Eq. 1. The Smith iterative (Smith, 1970) and Tikhonov regularisation (Tikhonov et al., 1990) methods were used for testing temperature retrievals from PFS radiance spectra. First, using the MARSGRAM software (Justus et al., 1995), three 'true' temperature profiles were selected, representing the variety of conditions on Mars: *1* equatorial day model; *2* equatorial night model; *3* polar summer model. The synthetic spectra of the outgoing radiation calculated for each temperature model and dust-free atmosphere are shown in Fig. 3.

Each retrieval algorithm organises its own process of iterative correction of the initial profile. It is done in different ways but all the methods tend to reduce the deviation of the synthetic profile from the 'measured' one.

The surface pressure is usually a free parameter in the retrieval procedures. However, the measurements in the 2.0 µm CO_2 band simultaneously carried out in the PFS short wavelength channel will provide the necessary data on the surface pressure, at least for daytime observations. So it was assumed that the surface pressure was known in this set of test retrievals.

Temperature profiles retrieved by the Smith iterative and Tikhonov regularisation methods are compared in Fig. 4 with the 'true' profiles. The retrieval error bars for dust-free tests are also presented in the right side of the figure. The following conclusions about the PFS temperature-sounding capabilities can be drawn from the test retrievals:

— in the dust-free atmosphere, the temperature profile can be retrieved from the measurements in the 15 µm CO_2 band with an accuracy of ~3K in the altitude region 0-65 km. This value can be considered as the noise of the retrieval procedures. The accuracy of the retrievals from the actual measurements will depend on the signal-to-noise ratio (S/N) achieved in the PFS measurements;
— the retrieval errors increase above 65 km because the weighting functions decrease with altitude (Fig. 2) and the radiance measurements are no longer sensitive to atmospheric temperature;
— the retrieval accuracy at the surface is 2-3K by deriving the surface pressure from the 2.0 µm CO_2 measurements. This was proved by several test retrievals with the wrong surface pressure;
— test temperature retrievals from the dusty spectrum without taking aerosols into account resulted in ~10K errors in the lower 10 km of the atmosphere.

1.3.4 The influence of aerosols

Dust is always present in the martian atmosphere. Its abundance varies significantly with season and from year to year. Its optical depth changes from 0.2 to more than unit in the visual range. The absorption features of palagonite dust were discovered in Mariner-9 spectra. In the short wavelength wing of the 15 µm CO_2 band, the water ice features have been found in Mars Global Surveyor/TES spectra. They were observed at high zenith angle, together with palagonite bands.

The influence of aerosols on martian spectra were modelled, assuming the presence of palagonite aerosols (optical parameters were taken from Roush et al., 1993) with modified gamma particle size distribution (Pollack & Toon, 1982):

$$n(r) \propto r^{\alpha} \exp\left[\frac{-\alpha}{\gamma\,(r/r_m)^{\gamma}}\right] \tag{3}$$

The modal radius $r_m = 0.4$, effective radius $r_{eff} = 1.6$ µm and constants $\alpha = 1$ and $\gamma = 1$ were used. In the spectral range favourable for temperature and aerosol retrieval, the single scattering albedo is less than 0.4; aerosol particles are black and non-scattering. In order to model the aerosol influence in the spectral range of temperature retrieval, spectra were calculated for optical depth $\tau = 0.3$, 1, 10, and scale height Ha = 10 km at zenith angles of observations 0° and 70°. The results are shown in Fig. 5.

The aerosol influence on the spectra can be summarised as:

— aerosol absorption increases the altitude of the effective emission level. So a temperature profile retrieved with pure gaseous transmission functions relates to the shifted levels;

— aerosol absorption can be asymmetrical in the wings of the 15 µm band. The absorption coefficient is doubled in the long wavelength wing. The measured brightness temperature in the short wavelength wing agrees with calculations, although in the long wavelength wing it is systematically lower.

1.4 The 3-D global atmospheric circulation

Direct observations of winds in the martian atmosphere are very rare, available for only a few landing sites. Wind direction and speed derived from cloud tracking and aeolian streaks correspond to the boundary layer and are often ambiguous (see Zurek et al., 1992, and references therein). Remote sounding from orbit remains the most valuable source of information about the large-scale dynamics of the atmosphere. Long-term global monitoring by PFS of such atmospheric parameters as vertical temperature profiles, aerosol optical depth, surface pressure and water vapour column density will provide an important insight into the following aspects of the atmospheric dynamics:

Global circulation. The fundamentals of atmospheric dynamics on rapidly rotating planets like Earth and Mars show that geostrophic winds derived from the remotely determined 3-D temperature field are a good approximation of the true large-scale atmospheric motions in a non-equatorial zone (Pedlosky, 1979). So far, thermal winds have been retrieved only from the Mariner-9/IRIS observations taken during the northern winter (Zurek et al., 1992). Long-term global temperature sounding of the martian atmosphere by PFS will have complete latitude, longitude and seasonal coverage in the altitude range from the surface up to about 60 km. This will allow us to determine systematically the wind pattern and to follow seasonal changes in global circulation. Simultaneous monitoring of the atmosphere's dust content will provide further insight into the role of dust in the atmospheric dynamics. PFS observations will also help us to understand the mechanisms of polar warming, which is supposed to be of a dynamical nature.

Wave phenomena. The experience gained from the analysis of Mariner-9/IRIS and Viking/IRTM data shows that similar observations of the atmospheric temperature field by PFS will allow us to study some important wave phenomena: thermal tides and their interaction with large-scale topography, quasi-stationary waves probably generated by instabilities in the mid-latitude zonal jet, and large-amplitude waves at high latitudes during the polar warming.

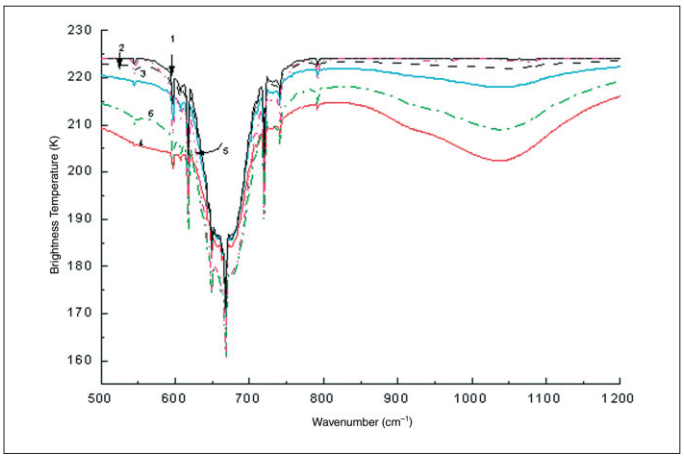

Fig. 5. Synthetic spectra of Mars' atmosphere, including the 9 µm palagonite absorption band.

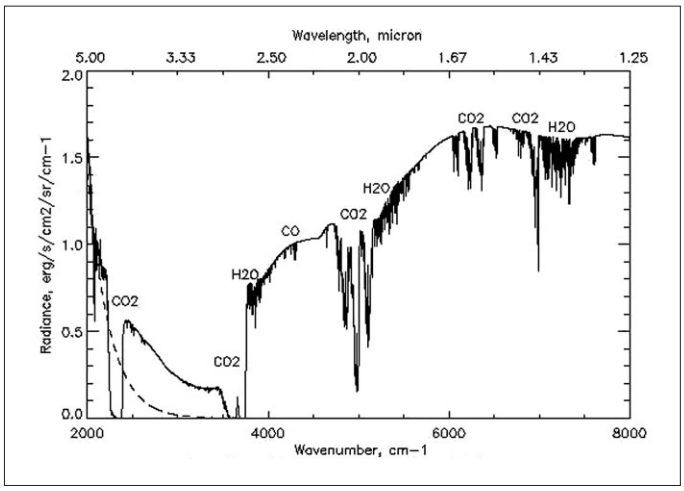

Fig. 6. Synthetic spectrum for the PFS SW channel.

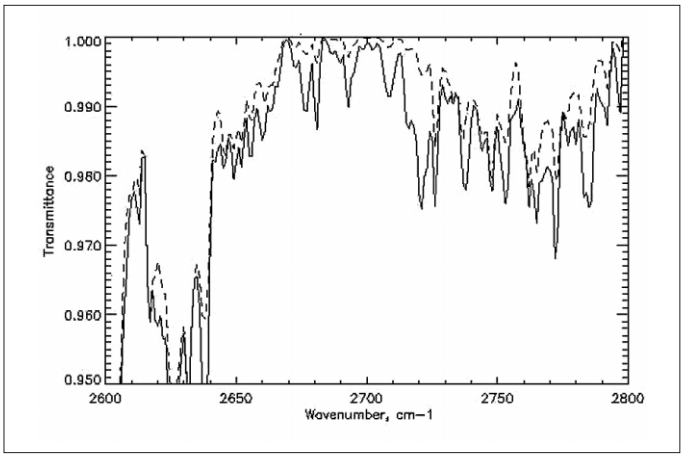

Fig. 7. Synthetic transmittance spectrum in the 3.7 µm HDO band.

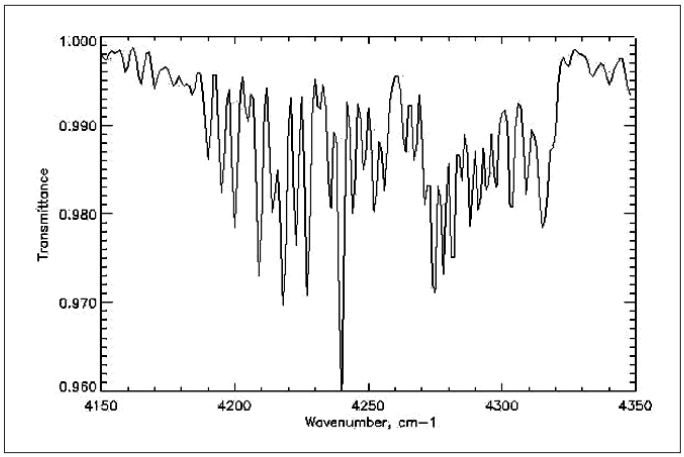

Fig. 8. Synthetic transmittance spectrum in the 2.35 µm CO band.

Transport of atmospheric species. Mars is a unique planet, where the main atmospheric component (carbon dioxide) is deposited on the polar caps in winter. This produces seasonal variations of up to 25% in surface pressure. Systematic measurements of this parameter by PFS will give an estimate of the mean meridional flow from summer to winter hemisphere. Furthermore, the water vapour that sublimes from the polar cap in summer and is then transported to the lower latitudes can be used as a tracer of the large-scale atmospheric motions (Haberle & Jakosky, 1990). PFS observations of atmospheric water will impose additional constraints on the transporting winds.

1.5 The minor constituents

Minor constituents identified in the atmosphere of Mars are H_2O, CO, O_2, O_3, He, Ne, Ar, Kr and Xe. Their mixing ratios are less than 10^{-3}. Four of these gases have bands in the PFS spectral range: H_2O, CO, O_3, O_2 (Fig. 1). The bands of isotopes such as HDO, $^{13}C\ ^{16}O_2$, ^{12}C, ^{16}O and ^{18}O are well separated from the bands corresponding to the main isotopes and may be used to re-estimate the isotopic ratios.

Synthetic spectra of Mars in the wide spectral range of 1.2-45 µm were computed

in order to analyse the PFS capabilities in the investigation of minor constituents.The general view of the martian spectrum in the near-IR range is shown in Fig. 6.

The spectrum demonstrates sharp absorption features of the atmospheric CO_2, H_2O and CO, and a broad spectral signature of surface minerals at ~3 μm. It also shows the contribution from thermal emission at $\lambda > 4$ μm (dashed line). The computations were performed for the nominal temperature model (mid-latitudes, northern summer) elaborated on the basis of Viking landing data (Seiff, 1982). PFS measurements will provide the H_2O detection limit of ~1 μm. The transmittance spectrum of HDO is shown in Fig. 7. Fig. 8 presents the CO transmittance spectrum for the mixing ratio of $6x10^{-4}$.

The martian volcanoes are the highest in the Solar System. They cover more than 2 atmospheric scale heights (~27 km in the case of Olympus Mons). Such topographical features offer the possibility of obtaining vertical profiles for trace gases and dust. PFS observations along the slopes will sound increasingly high altitudes as the field of view moves towards the top. However, the analysis of such observations is not straightforward because the vertical profiles of the species in the vicinity of the slopes can be affected by the surface-atmospheric interactions and can differ from those in the free atmosphere.

1.6 Water distribution and cycle in the martian atmosphere

The first detection of H_2O on Mars was made by Earth-based spectral observations at high resolution (about 0.1 Å) using the Doppler shift of weak lines with respect to much stronger telluric features in the band at 8200 Å (Spinrad & Richardson, 1963; Kaplan et al., 1964). If a telluric absorption line is not oversaturated, then a much weaker planetary feature belonging to the same gas can be visible on its wing because of Doppler shift. Water vapour in the martian atmosphere have been studied systematically using this method, including average abundance and latitude, daily and seasonal variations. Average water abundance of about 10 μm ppw (precipitable microns water equivalent) is a typical value. However, the ground-based observations had intrinsic limitations in spatial resolution and coverage.

Measurements of water bands in the atmosphere of Mars were also performed by several experiments onboard the orbiters Mars-3 (Moroz & Nadzhip, 1975), Mariner-9 (Hanel et al., 1972) and Viking-1 & -2 (Jakosky & Farmer, 1982). These experiments provided much better spatial resolution ($\leq$ 20 km) and detection threshold (1-3 μm ppw).

Mariner-9/IRIS detected atmospheric water vapour in the region from the South Pole to the Equator, using rotational lines in the spectra between 250 cm^{-1} and 500 cm^{-1}. These features were not observed over the North Pole. The total amount of water vapour in the atmosphere was estimated from a quantitative comparison of observed and synthetic spectra in the range 10-20 μm ppw. It has been proposed (e.g. Pollack et al., 1979) that water vapour abundance in the atmosphere may be greatly affected by the adsorption of water vapour on dust particles. Suspended dust particles would supply a large surface, producing rather efficient adsorption. Much of the water vapour would settle with dust and it would be released again into the atmosphere as the temperature increases. There is a strong coupling between the temperature and the water abundance fields, but there is still no clear understanding of all the possible sources and sinks of atmospheric water.

Sublimation of water from the north polar cap certainly occurs, but the best model is still uncertain on the quantity. Similarly the regolith is certainly capable of adsorbing and desorbing water, thereby modulating to some degree the amount of water within the atmosphere. The efficiency of this process depends, however, on the composition of the regolith and on the ability of water molecules to diffuse through the uppermost centimetres of regolith, and both of these are very uncertain (Jakosky & Haberle, 1992). A set of experiments on future Orbiters and Landers is necessary for a real understanding of the seasonal cycle. First of all, long-term studies (many martian years) of water vapour are necessary. Several missions are required and PFS will make a crucial contribution.

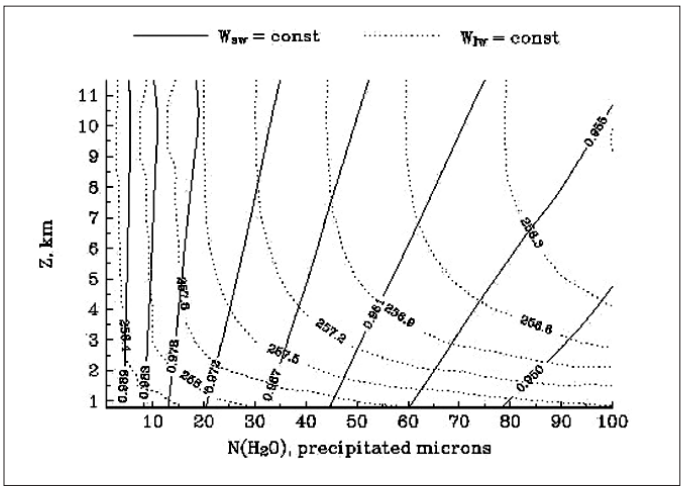

Fig. 9. Simultaneous measurements of the equivalent width of two H_2O bands gives information about the vertical distribution of water vapour.

The water vapour mixing ratio profile seems to indicate the existence of two regions in the atmosphere: below 20-25 km there is relatively high water abundance; above this boundary, it is about 10 times lower (Rodin et al., 1997).

Three different spectral ranges could be used for remote measurements of atmospheric water from orbit:

— near-IR: bands at 1.38, 1.87, 2.7 μm;
— thermal-IR details of the pure rotational H_2O band in the range 20-50 μm;
— microwave lines of the pure rotational bands (1.63 μm, for instance).

The sensitivity curve of PFS is such that the 1.87 μm and 2.7 μm bands are more favorable. The detection threshold of 1 μm ppw could be achieved in measurements with an S/N of 100.

The 1.87 μm band appears to be the most convenient for H_2O detection, as it is almost free of overlap with the CO_2 bands. However, the 2.7 μm band will be used to make the H_2O abundance determination more accurate.

The disadvantage of the thermal-IR range is the strong dependence of the water spectral features on the temperature profile in the lowest 1-3 km of the atmosphere, which cannot be resolved directly by any remote-sounding experiment. In principle, we can observe H_2O features in the thermal-IR range not only in absorption but even in emission (in the case of the temperature inversion just above the surface). However, the joint analysis of the H_2O spectral details observed simultaneously in the near-IR and in the pure rotational bands can impose constraints on the vertical distribution of water vapour. Fig. 9 shows the isolines of equivalent widths of the 1.87 μm band (solid lines) and 50 μm band (dots). This diagram is based on a set of calculations of synthetic spectra for various H_2O vertical profiles. The abscissa shows the H_2O column density and Z is the effective altitude of water location. Fig. 9 demonstrates that simultaneous measurements in several water vapour bands will be able to give an estimate of vertical distribution.

PFS also provides an additional opportunity for detection of the 3.7 μm HDO band. It was observed in the martian spectrum by Owen et al. (1988) and the D/H ratio was found to be considerably higher than on Earth (about 6 times). PFS could provide a new, independent determination of this ratio.

In summary, PFS will perform long-term observations of atmospheric water vapour on Mars. This will provide further understanding of the behaviour of water on the planet, its seasonal and diurnal cycles, and distribution of sources and sinks. In comparison with other experiments that have measured martian H_2O, PFS has several advantages:

— the uncertainties in temperature profile, which are usual for near-IR observations of water vapour bands, will be minimised by simultaneous temperature-sounding in the 15 μm CO_2band;
— high spectral resolution in the near-IR range will result in clear discrimination between the atmospheric and surface spectral features, making the quantitative analysis more reliable;
— simultaneous observations of the water vapour bands in thermal-IR and near-IR will help the vertical distribution of H_2O to be estimated.

1.7 The aerosol investigation

1.7.1 Introduction

The scientific objectives of PFS include:

— the determination of the optical properties, size distribution and chemical composition of the atmospheric aerosols: dust clouds, ice clouds and hazes;
— the investigation of the influence of aerosols on energy exchanges in the atmosphere.

The surface-atmosphere interaction plays a role in the surface's morphology and chemical composition and the atmosphere's temperature, pressure and composition. It is well known that the CO_2, water and dust cycles are strongly interconnected and with the seasonal variations. Winds, erosion processes and global dust storms are the principal mechanisms for material exchange between aerosols and the surface and between different regions of the planet. Studying the atmosphere's solid components is therefore an important task. Furthermore, the composition of the atmospheric dust provides clues on the chemical composition of the surface, because the identification of dust materials implies characterisation of the soil properties. Last but not least, correctly interpreting the atmosphere's pressure and temperature behaviour must include the role played by the aerosols.

1.7.2 The dust cycle

Atmospheric dust has a role in determining the martian climate and it is clear that it is key for surface geology over a long time scale.

Suspended dust affects the thermal structure and atmospheric circulation with a typical seasonal evolution (Haberle, 1986). The increase of opacity in the northern hemisphere autumn and winter is consistent with global dust storms. This effect is linked to the planet's perihelion, when heating and atmospheric circulation reach maximum. Atmospheric opacity also depends on the form, dimension and composition of the dust grains.

During local dust storms, the lifted materials are redistributed over contiguous areas, while global dust storms transfer dust from the southern hemisphere to the north and the polar cap. Beside the storm effects, dust can be transferred through the atmosphere by baroclinic and planetary waves (Kahn et al., 1992). The dust is probably placed in suspension by strong winds and/or water and CO_2 degassing from the regolith.

The continuous monitoring of the martian atmosphere by PFS in the IR will reveal the evolution of the aerosol composition and amount. Moreover, the dust cycle is strongly linked to the water and CO_2 atmospheric cycles. In fact, the presence of dust at the poles can significantly affect the energetic balance and, then, influence the water vapour and CO_2 fluxes. Dust grains in the atmosphere may become condensation nuclei for CO_2 and H_2O accretion on their surfaces. In particular, the CO_2 condensed on the grain surface may act as a cold trap for atmospheric water. In addition, the transfer of dust from the surface to the atmosphere depends on the pressure and, therefore, on the CO_2 abundance. These elements are further evidence that dust and gas composition of the atmosphere are connected and cannot be treated separately.

1.7.3 Aerosol dust particles

Although spectral signatures of dust particles were clearly evident in Mariner-9/IRIS spectra, it was difficult to define the bulk composition of solid grains with a high degree of confidence. The content of SiO_2 in the dust has been inferred from the comparison of observations with laboratory data; it appears to be 60±10%. Phobos-2 observations of the martian atmosphere using solar occultations in the UV and visible revealed absorption features, probably owing to aerosols (dust particles interpreted as haematite-type) and ozone. A correlation seems to exist between the amount of particulate material in the atmosphere and ozone abundance. This evidence suggests the possibility of heterogeneous chemistry in martian aeronomy (Atreya, 1989) and confirms that aerosols and dust particles play an important role in atmospheric evolution. However, the nature of the particles and their size distribution is not well determined. Atreya (1989) suggests that they could be ices covered by different types of dust (haematite, magnetite and limonite). The PFS data will be helpful in identifying the aerosol nature: the spectrum of light scattered by the atmospheric particles and their thermal emission are sensitive to the chemical composition and size distribution. Additional restrictions could be imposed by the phase function measured by PFS. The problem of separating contributions from the surface and atmospheric radiation should be solved when the aerosol optical depth is not very large. PFS will provide the opportunity for simultaneous measurements of the spectra of the scattered light and the thermal emission of clouds and hazes in the wide range 1.25-45 µm.

1.7.4 The composition of dust

The wavelength range of PFS over 5 µm can be diagnostic for the composition of dust. Much observational evidence indicates the presence of silicate materials, but attribution to a specific class has not yet been achieved. The Mariner-9 data suggested that montmorillonite might be a major component (Hunt et al., 1973). While the observed 10 µm silicate band is easily reproduced by laboratory spectra of crystalline clays, problems occur in simulating the 20 µm band: it does not exhibit any double peak, as is typical of many terrestrial silicate materials. Further observations by PFS at 10 µm and 20 µm could reveal spectroscopic details helpful for identifying the silicate minerals in martian dust. Thermal emission spectra of Mars in the 5-10 µm range have been obtained by a grating array spectrometer aboard the Kuiper Airborne Observatory (Pollack et al., 1989). The observations confirmed that the spectrum of Mars at > 5 µm has more features than previously believed (Roush et al., 1989). Features at 6.1, 7.8 and 9.8 µm are attributed to water and silicate minerals on the surface. Weaker features appear atmospheric in origin: the CO_3^{2-} anionic group can contribute with bands at 6.7 µm and 7.05 µm, when included in distorted sites of complicated crystalline structures; and SO_4^{2-} and HSO_4^- in sulphates and bisulphates produce resonances at 8.7 µm and 9.78 µm. Again, there are doubts about the relative amount of carbonates and sulphates in the form of dust. PFS observations could provide details on cation composition in complex crystalline materials.

1.8 The soil of Mars

1.8.1 Introduction

The spectral studies of the martian surface indicate there to be different types of soil and rocks. They include drift soil, which is similar to the global dust and already analysed by remote spectral measurements from Mariner-9/IRIS, Viking and Phobos-2/ISM and directly at the Viking and Pathfinder landing sides by X-ray fluorescence (Toulmin et al., 1977). There is also sand – attributed to local weathering processes – and more crystalline soil that could be a mixture of dust and local material. The Pathfinder landing site is dominated by three rock types. Dark rocks such as Barnacle Bill and Bambam seem to be fresh basalt or basaltic andesite (Rieder et al., 1997). Bright rocks like Broken Wall and Wedge are attributed to weathered basalts or basaltic andesite. Pink rocks are thought to be chemically cemented drift formations. There is clearly a wide variety of chemical, mineralogical and

morphological characteristics in the surface material at the site. Global spectral studies by PFS will add information on how representative these features are for the whole surface, by comparing the PFS observations of the Pathfinder site with other martian targets. Mapping the distribution of hydrated minerals and salts in the soil is important for understanding the weathering processes and the former role of water on Mars.

1.8.2 The role of PFS

To study the surface of Mars, PFS observations will address the following objectives:

— thermal measurements and determination of the soil's thermal inertia;
— evaluate the local atmospheric pressure and the relative altitude of various regions;
— overview of generic areas of the surface in order to trace the overall distribution of various materials (iron oxides, clays, palagonites, hydrates, sulphates, nitrates, igneous minerals, ices);
— study specific areas chosen to search for answers to fundamental questions on the evolution of the planet and the ancient paleoclimate, e.g. the past existence of abundant liquid water on the surface (by searching for carbonates and other evaporites);
— study the surface-atmosphere exchange processes.

IR spectroscopy in the range covered by PFS is a powerful tool for exploring the surface composition. Different families of resonance fall within the IR spectral range:

— charge transition bands of electrons in the lattices of transition metal ions;
— charge transfer bands due to electron exchange between ions in the material;
— vibrational bands of radicals/molecules present in minerals.

In general, discriminating between atmospheric and surface contributions to the spectrum is rather difficult, requiring a combined study of surface and aerosol/dust constituents. Correctly interpretating the gaseous atmospheric composition requires the subtraction of the solid material's contribution from the recorded spectra.

Finally, a quantitative identification of materials must be based on a comparative analysis of the collected spectra with laboratory measurements on analogue compounds representing martian materials.

1.8.3 Determination of the thermal inertia of the soil

Thermal inertia, which depends on thermal conductivity, mass density and specific heat, is a measure of the responsiveness of a medium to changes in its temperature. The dominant reason for variations in thermal inertia is generally grain-size differences in the superficial material. Thus data on thermal inertia have the potential for telling us if the superficial material is relatively coarse- or fine-grained.

Using PFS measurements of the thermal spectrum from the martian surface in the wide spectral range 5-45 µm, it is possible to determine the pre-dawn temperature of the soil and, from this, its thermal inertia. This can be done by comparing the actual pre-dawn temperatures with those predicted by an idealised thermal model of the surface layer (Kieffer et al., 1977).

1.8.4 Evaluation of the local atmospheric pressure and elevation

The depth of the carbon dioxide unsaturated absorption band measured at a specific site depends on the local atmospheric pressure and, consequently, on the altitude . The PFS SW channel (1.2-5.0 µm) could be used to acquire pressure and relative elevation data and, finally, to map the surface relief. Such an approach was applied to the Mars-3 and -5 and Phobos data.

1.8.5 The chemical and mineral composition of the surface

Among the prime unresolved and oft-debated questions of Mars is the structure and composition of its surface materials. Reflectance and emittance spectroscopy in the near-IR and mid-IR is diagnostic of mineralogy, and hence provides useful information on the surface composition. The spectra of minerals in terrestrial conditions show remarkable dependence on varying experimental situations, including the form of the material (which may be bulk or particulate with different granularity and packing), background temperature, uniformity of sample heating, pressure and insolation angle.

1.8.6 Iron oxides

Crystalline ferric oxides, such as haematite, have long been proposed as one of the major components of the martian surface, in view of the planet's colour and the substantial amount of Fe_2O_3 measured in the soil by the Viking Landers. The broad absorption bands around 10 µm and 20 µm, observed in the spectra from Mariner-9/IRIS, appear inconsistent with crystalline ferric oxides. On the other hand, there is no evidence for such compounds at the Pathfinder site.

The comparisons performed so far with the spectra of Mars suggest that either only a few percent of coarsely crystalline haematite or abundant but nanocrystalline haematite are present in the studied areas (Morris & Lauer, 1990). However, a more systematic research of spectral features typical of Fe^{3+} resonances on the martian surface can be useful to clarify this point. Spectroscopic observations by PFS in both SW and LW channels (where haematite shows narrow bands at 2.9, 6.1 and 7.8 µm and broad bands around 18.5 µm and 21.5 µm) can be a great help in determining the main allotropic form of haematite on Mars. The spectral resolution of PFS in this case should have a strong diagnostic power, since the spectral bands of samples with a high degree of crystallinity are, in general, more structured than those of nanocrystalline or amorphous samples (which tend, instead, to be structureless).

1.8.7 Water in the martian soil

PFS will also trace the distribution of hydrates on the surface, by analysing the H_2O bands around 3 µm (due to O-H stretching) and around 6 µm (H-O-H bending). Although it is clear that hydration water is widespread on the surface, there is not much of it. Surface materials should, in fact, be dehydrated in comparison with terrestrial soils, with a water content of up to a few percent (Soderblom, 1992). PFS can improve, on a statistical basis, these evaluations by searching for regions with a higher content of hydration water.

1.8.8 Ices

Mars has a dynamical seasonal cycle of CO_2 and H_2O exchange between the surface and atmosphere. The interplay between vaporisation and condensation of both CO_2 and H_2O produces clouds and mists in the atmosphere and frost and ices on the surface. We expect – apart from polar summers – that PFS observations of ice and frost deposits may be hindered by clouds and mists.

As the role of H_2O in the polar cycles remains to be clarified, searching for CO_2 and H_2O ice and frost features in the spectra of the north polar region will be very useful. Unlike H_2O ice, which strongly absorbs throughout the thermal-IR, CO_2 ice absorbs strongly in the bands at 2.7 µm, 4.3 µm in the SW channel of PFS and at 15 µm in the LW channel. This difference could be a basis for distinguishing between the two substances while observing the surface ice deposits. If, however, there are abundant particles of solid CO_2 more than a few µm in size, as there probably are at the polar caps, the reflectivity and emissivity of the surface deposits are also strongly influenced by the weak absorption between the strong bands (Hansen, 1997). In such conditions, a thorough examination of these spectral regions is important.

2. Instrument Description

2.1 Introduction

PFS is a double pendulum interferometer working in two wavelength ranges (1.2-5 µm and 5-45 µm; Table 2). Martian radiation is divided into two beams by a dichroic mirror. The two ranges correspond to two planes (one on top of the other) containing the two interferometers, so that the same motor can simultaneously move the two pendulums and the two channels are sampled simultaneously and independently. The pendulum motion is accurately controlled via a laser diode reference channel using the same optics as the martian radiation. The same laser diode also generates the sampling signal for the analogue-digital converter (ADC), measuring the 600 nm displacements of the double pendulum mirror. The measurements are double-sided interferograms, so that the onboard FFT can be computed without needing the zero optical path difference location.

2.2 Instrument organisation

PFS is a Fourier spectrometer produced by the combined efforts of several groups from Italy, Russia, Poland, Germany, France and Spain. The flight hardware was built in Italy (the Interferometer Block with its controlling electronics, the digital electronics controlling the experiment, and the Ground Support Equipment with the spacecraft simulator) and Poland (power supply and pointing system). Special flight parts and subassemblies were built in Russia and Germany.

2.3 Technical description

The flight hardware, totalling 31.2 kg, is divided into four modules (Fig. 10), with connecting cables (0.8 kg):

— Module-O (PFS-O): the interferometer, with its optics and proximity electronics, is the core of PFS. 21.5 kg;
— Module-S (PFS-S): the pointing device, which allows PFS to receive radiation from Mars or from the inflight calibration sources, 3.7 kg;
— Module-E (PFS-E): the digital electronics, including a 32-Mbit mass memory and a realtime FFT. 3.0 kg;
— Module-P (PFS-P): the power supply, with the DC/DC converter, redundancies and the separate power supplies for the 16-bit ADCs. 2.2 kg.

Power requirements are: 5 W thermal control, 10 W in sleep mode, 35 W full operational mode and 44 W peak.

2.4 Module-O (PFS-O)

PFS-O is divided into the Interferometer Block (IB) and Electronics Block (EB). They are mechanically separated but electrically connected through six cables. The highly compact IB is a gas-tight box filled by dry nitrogen in order to preserve the hygroscopic optical elements.

2.4.1 Optical scheme of PFS-O

The optical scheme of PFS is shown in Fig. 11. The incident IR beam falls onto the entrance filter that separates the radiation of the SW channel from that of the LW channel and directs each into the appropriate interferometer channel. The PFS-S in front of the interferometer allows the FOV to be pointed along and across the projection of the flight path onto the martian surface. It also directs the FOV at the internal blackbody sources diffusers and to open space for inflight calibration. Each PFS channel is equipped with a pair of retroreflectors attached by brackets to an axle rotated by a torque motor. The axle and drive mechanism are used for both channels, which are vertically separated. The optical path difference is generated by the rotation of the retroreflectors (Hirsch & Arnold, 1993). The motor controller uses the outputs of two reference channels, which are equipped with laser diodes. This interferometer design is very robust against misalignment in a harsh environment, in comparison

Table 2. PFS characteristics.

	SW	*LW*
Spectral range, μm	1.2 – 5.0	5 – 50
Spectral range, cm^{-1}	2000 – 8200	250 – 1750
Spectral resolution, cm^{-1}	1.5	1.5
FOV, deg	1.7	2.8
NEB, W cm^{-2} sr^{-1}	5×10^{-9}	4×10^{-8}
Detector type	photoconductor	pyroelectric
Material	PbSe	$LiTaO_3$
Temperature, K	220	290
Interferometer type	double pendulum	
Reflecting elements	cubic corner reflectors	
Beamsplitter	CaF_2	CsI
Max. optical path difference, mm	5	5
Time for motion, s	5	5
Reference source	laser diode	
SW/LW separation	KRS-5 with a multi-layer coating reflecting SW radiation	
Interferogram	two-sided	
Sampling number	16384	4096
Sampling step, nm	600	600 (over-sampled)
Dynamical range	2^{15}	
Spectra (from onboard FFT), number of points	8192	2048

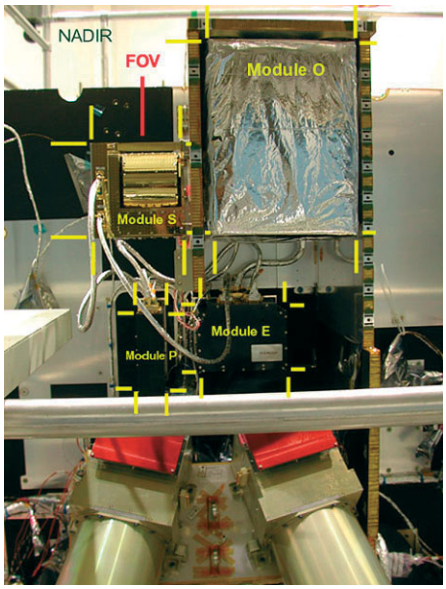

Fig. 10. PFS Flight Model integrated on Mars Express at prime contractor Alenia Spazio in Turin.

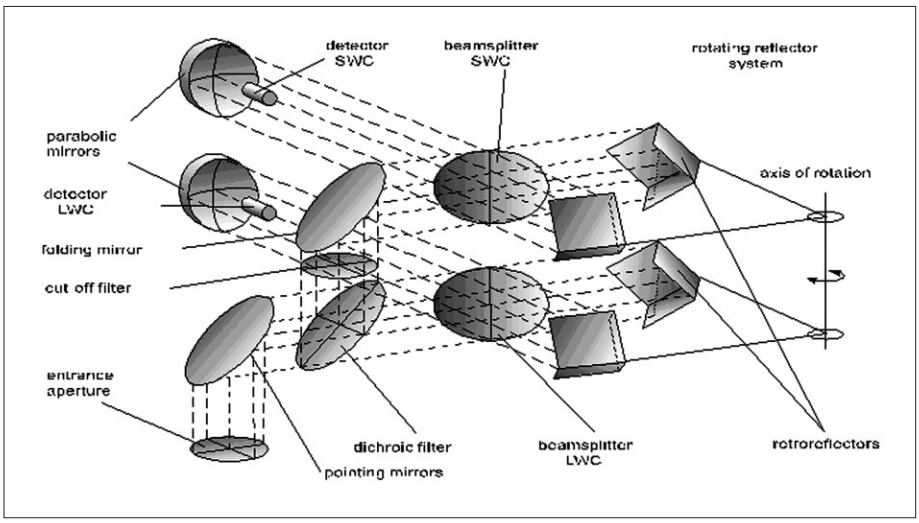

Fig. 11. PFS optical scheme.

with the classical Michelson-type interferometer (Hirsch, 1997). The detectors are in the centre of the parabolic mirrors. The optical path is changed by rotating the shaft of the double pendulum along its axis. In this way, the optical path is four times that provided by a single cube-corner displacement because two mirrors move at the same time. The dichroic mirror acts as a fork that divides the two spectral ranges. Indeed, it reflects all the wavelengths below 5 μm and remains more or less transparent for longer wavelengths. The band stop for wavelengths below 1.2 μm is provided by the silicon window, with its cutoff at 1.24 μm and placed in the optical inlet of the SW

channel. This filter is tilted by 1.5° so that the radiation returning to the source is not partially reflected on the detector.

The double-pendulum axis is rotated by a brushless, frictionless motor (two for redundancy). The shaft of the double pendulum is held only by two preloaded ball bearings so additional mechanical friction is required for stabilising the pendulum speed.

Double-sided interferograms are acquired by placing the zero optical path difference in the centre of the mirror displacement. A double-sided interferogram has several advantages, including a relative insensitivity to phase errors. Bilateral operation is adopted in order to reduce the time-cycle of each measurement, but separate calibration for each direction is recommended in order to maintain the radiometric accuracy.

The spectral reference beam is a diode laser (InGaAsP at 1.2 µm); its detector is an IR photodiode with maximum response at about 1.2 µm. The beam of the reference channel is processed like the input signal so that its optical path coincides with that of the signal being studied. Each channel has its own reference beam and the different lengths of the double-pendulum arms are fully compensated for. Because the LW beam splitter is not transparent at the wavelength of the corresponding reference diode laser, a special small window was added in order to keep the attenuation of the laser beams negligible through the beam splitter itself. The unused output beams of the two reference channels terminate into optical traps.

2.4.2 Electronics of PFS-O

Most of the electronics inside PFS-O are analogue but the microprocessor-based On-Board Data Management (OBDM) board controls all the complex procedures during acquisition of the interferogram, including communication with PFS-E. It includes 32 kword of EPROM for software storage and 96 kword for data. The most important electronics block is the speed controller. The zero crossing of an interferogram of a monochromatic source that is very stable in wavelength can be used for sampling the interferogram of the source under study. Ideally, the interferogram of the monochromatic source should be a pure sine wave but it is not simply because its interferogram is limited in time. The shorter the wavelength of the reference source means better sampling accuracy.

For PFS, 1.2 µm is the reference source because of the limited variety of diode lasers and it simplifies the optical design. The wavelength of a diode laser depends on its temperature and power, so great care has to be taken in their control.

The speed of the double pendulum is such that a frequency of 2 kHz is generated for the SW channel, so a train of 4 kHz pulses is produced from the electronics of the SW reference channel. Thermal control is also very important for an IR interferometer; heaters and thermometers are positioned at eight locations.

A ‘locking system’ blocks the double pendulum during launch and manoeuvring for orbital insertion and correction. The procedure of locking and unlocking takes a minimum of 3 min but using a paraffin actuator means it can be repeated hundreds of times. The launch acceleration vector will be along the axis of the double pendulum for maximum robustness.

The photoconductor SW channel detector can work at temperatures down to 200K. It is passively cooled through a radiator and its holder is partially insulated from the rest of the IB. For the LW channel, the pyroelectric detector can operate without performance degradation even at ambient temperatures.

2.5 Module-E (PFS-E)

PFS-E controls all the PFS modules: the communications to and from the spacecraft, memorising and executing the command words, and operating PFS and sending back the data words to the spacecraft. Moreover, it synchronises all the procedures according to the time schedule and to the clock time from the spacecraft.

2.6 Module-P (PFS-P)
PFS combines many kinds of electrical energy consumers: standard digital and analogue electronics, sensitive preamplifiers and ADCs, light sources and electromechanical devices (motors and relays). All of them have different supply requirements and some need to be electrically isolated (to ensure extremely high stability) and/or individually controlled by Module E's processor. This is why PFS-P is more complicated than a simple DC/DC converter: there are three independent converters, six different power outputs (totalling 13 independent voltages), one common input interface to satellite and one interface to DAM. All converters have cold redundancy. Switching between main/reserve +5 V is controlled by the spacecraft, while the other main/reserve converters are controlled by PFS itself.

2.7 Module-S (PFS-S)
The previous version of the pointing system, for the Mars-96 mission, had two degrees-of-freedom in pointing (two rotation axes), but was rather heavy (8.5 kg for the system and 2.3 kg for the controlling electronics). The pointing system is certainly necessary for generating a complete set of measurements, since we need to measure not only the martian radiation but also the calibration blackbody and empty space. Mars Express provides nadir pointing so PFS itself needs only one degree of rotation, simplifying the PFS-S design and reducing mass considerably (to 3.7 kg).

2.8 Modes of operation, data-acquisition cycle
PFS-S and PFS-O work in parallel during an observation session, while PFS-E coordinates operations of the other modules by sending commands and receiving messages. During measurements, PFS-S must be motionless while PFS-O acquires data. This is the only synchronisation point in the data-acquisition cycle. Upon completion of acquisition, all the modules work asynchronously while PFS-E coordinates their operations:

— starts rotation of PFS-S;
— receives LW and SW interferograms from PFS-O;
— if spectra are required, PFS uploads previously acquired LW and SW interferograms into the Fast Fourier Transform processor and downloads computed spectra;
— prepares the telemetry data pack i.e. splits information into frames and stores them in the mass memory;
— upon completion of the PFS-S rotation gives a command to PFS-O to start new acquisition.

After each data-acquisition cycle, PFS checks whether new telecommands have been received and, if any, executes them. Telemetry can be sent at any time on request from the spacecraft.

2.9 Inflight calibration
During observation sessions, PFS periodically performs calibrations by sending commands to PFS-S to point sequentially at the calibration sources: deep space, internal blackbody and calibration lamp. The housekeeping information obtained from PFS-O after each calibration measurement contains, in particular, the temperatures of the sensors and the blackbody. These data are used for the computation of the absolute spectra for the LW channel.

3. Test and Calibration

3.1 What is measured
The two detectors of the LW and SW channels measure the light intensity of the two interferograms. The repetition of the measurement while the double pendulum moves at constant speed gives the interferogram. In order to compute the spectrum from the

interferogram, the measurements must be taken at constant optical path difference, information given by the zero crossings of the sine signal from the interferogram of a monochromatic light (the laser diode).

3.2 Responsivity and signal-to-noise ratios

Three PFS models passed through the laboratory 'calibration' process: PFS-06 (Qualification), PFS-07 (Flight) and PFS-08 (spare FM, the refurbished PFS-06). 'Calibration' in this context means laboratory studies of the instrument properties that are necessary (although perhaps not sufficient) to extract spectra in absolute units from the observations of Mars by PFS. Ideally, calibrations should result in the algorithm of transfer from telemetric information to spectra of Mars in absolute units. However, instrument properties are not constant with time and the problem is complicated by the differences between laboratory and space conditions. Additional information, including inflight calibration and even models of martian spectra, is necessary for processing actual data.

Having a set of n independently found $B_{\nu^0}(i)$ spectra, we can compute the average spectrum $\mathbf{B}_{\nu^0}$ and noise equivalent brightness (NEB)

$$\mathrm{NEB}_\nu^2 = \sum \frac{B_{\nu^0}(i) - \mathbf{B}_{\nu^0}}{n - 1} \tag{4}$$

A more detailed discussion of the processing procedure for IR spectrometer data is given in Hanel et al. (1992). Two blackbody-imitator sources (cooled by liquid nitrogen) were used to study the PFS LW channel properties; one blackbody at 1400K was used to study the SW channel. Sensitivity D_ν and noise equivalent brightness NEB_ν were then computed from these measurements. The spectral resolution was measured with a mercury lamp and taking spectra with known features.

Fig. 12 shows the measured spectrum of the lamp used for calibrating both channels. The S/N is also computed from the measurements. Fig. 13 shows a CH_4 feature as measured in the LW and at maximum spectral resolution, to indicate that 2 cm^{-1} was achieved.

Rough computations show that an S/N at Mars of about 100 or larger will be achieved in the vicinity of 15 µm bands with the detector at 220K. This is good enough for retrieving the vertical temperature profiles of the atmosphere. Further studies of the instrument's thermal behaviour will be performed.

The responsivity for wavenumbers $\nu > 5000$ cm^{-1} is rather poor, because the reflectivity of the semi-transparent mirror separating LW and SW radiation is too low in this part of spectra. It is also this part of the spectrum where errors in optical alignment have greater impact. The situation is improved by optimising the transfer function of the SW channel filter.

3.3 Sample of performed measurements

Laboratory measurements were made on gases such as CO_2 by using a gas cell, and studying the transmission of radiation from a source. Fig. 14 shows the LW spectra around 15 µm, obtained for different CO_2 pressures inside the cell. Measurements were made at room temperature. Figs. 15 & 16 show the SW CO_2 band at 4.3 µm and 2.7 µm. It is evident that the spectral resolution allows the observation of rotovibrational features of the gas.

4. Data-taking Along the Orbit

4.1 Data-transmission modes

The data-transmission mode (DTM) defines the kind of scientific data that PFS must select and store in the mass memory to be sent to Earth. PFS has 15 DTMs, numbered for historical reasons, 0, 2, 4, 5, 6, 7, 8, 17, 18, 27, 28, 9, 10, 15, 16. DTM 0 is for PFS operating in the autonomous test mode; the others are obtained in the science

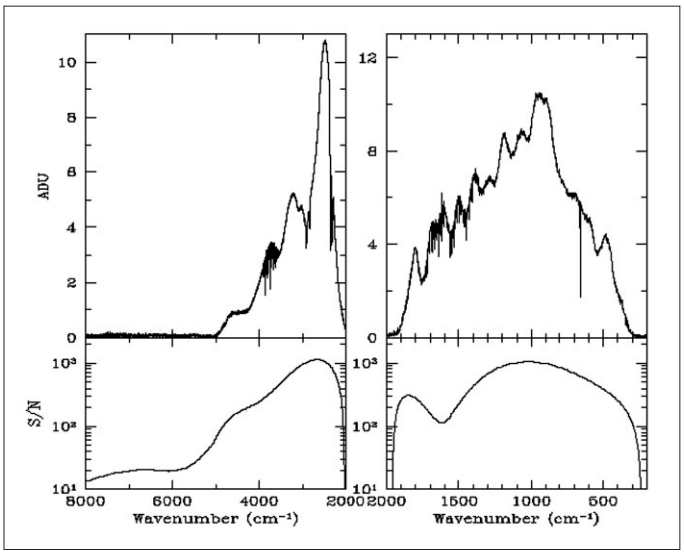

Fig. 12. Computed S/N for SW and LW using a single globar lamp spectrum.

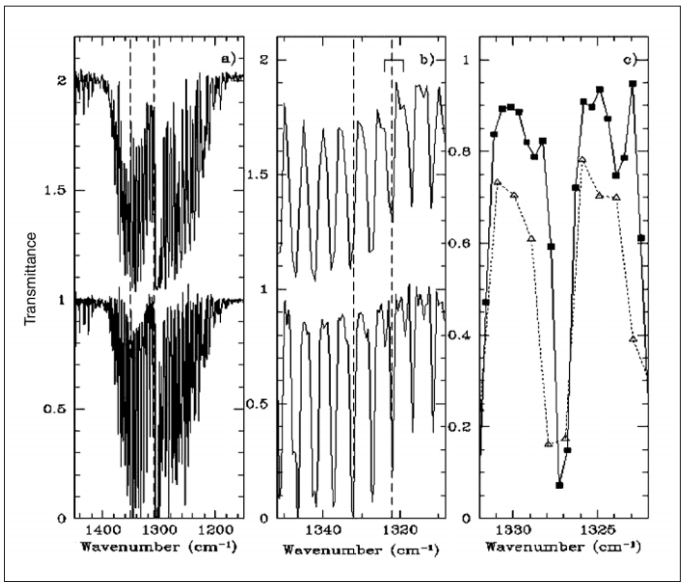

Fig 13. CH_4 bands in the LW channel at different resolution (PFS measurements: triangles; laboratory spectrometer: squares).

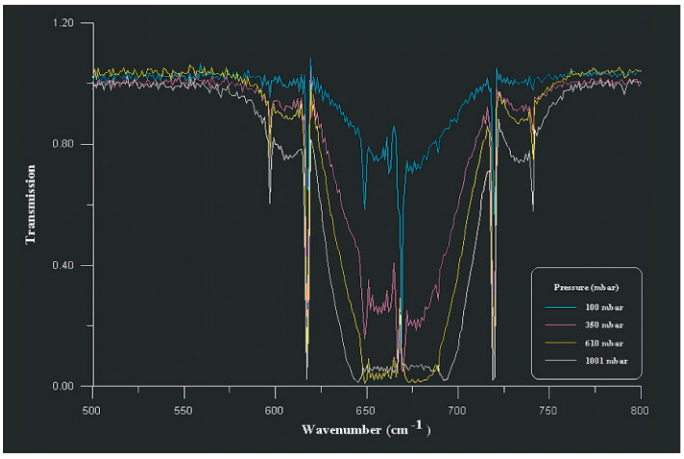

Fig. 14. CO_2 15-micron transmission band measured in the laboratory with PFS at different gas pressures.

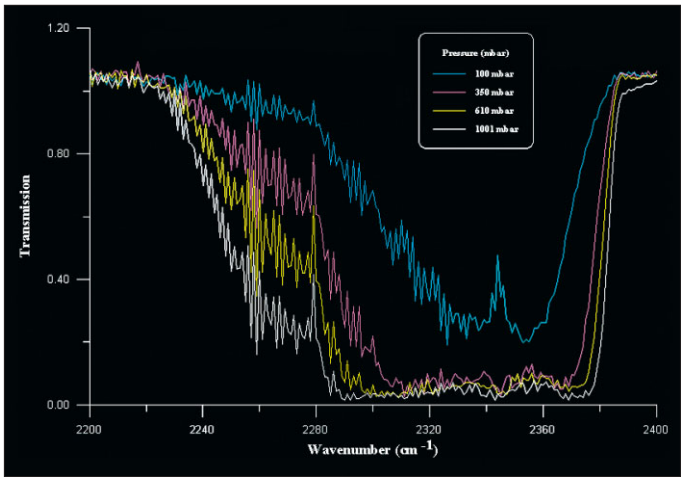

Fig. 15. CO_2 4.3-micron band measured with PFS in the laboratory at different gas pressures.

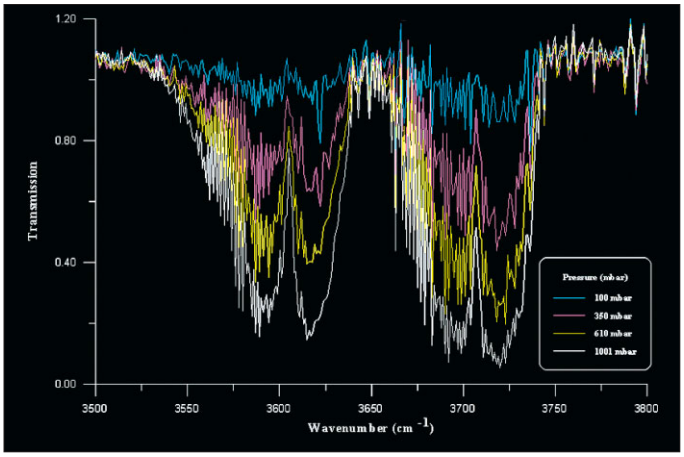

Fig. 16. CO_2 2.7-micron band measured with PFS in the laboratory at different gas pressures.

mode, where PFS acquires both LW and SW interferograms. If spectra are required (DTM 9, 10, 15, 16), PFS makes Fast Fourier Transforms of the interferograms. Then, depending on the DTM, PFS selects the required data. Interferograms can be selected completely or partially.

Of the 15 DTMs, 10 provide interferograms and four spectra:

- MODE 0: autotest of the interferometer (4096 points in the LW channel and 16384 points in the SW channel provide the sine wave shape and the monitoring of the speed during the double pendulum motion);
- MODE 2: full LW interferograms;
- MODE 4: half-resolution interferograms, SW and LW;
- MODE 5: half-resolution LW interferograms;
- MODE 6: half-resolution SW interferograms;
- MODE 7: full LW interferogram + one-sided SW interferogram (including the zero optical path difference and right side);
- MODE 8: one-sided LW and SW interferograms (right side);
- MODE 17: full LW and SW interferograms;
- MODE 18: full SW interferograms;
- MODE 27: full LW interferogram + one-sided SW interferogram (including the zero optical path difference and left side);
- MODE 28: one-sided LW and SW interferograms (left side);
- MODE 9: modules of LW and SW spectra;
- MODE 10: modules of LW spectra;
- MODE 15: full modules of LW spectra and SW spectra with reduced range (2000 points in the SW channel between 2000 and 4000 cm^{-1});
- MODE 16: modules of SW spectra (6144 points).

4.2 Data-taking along the orbit.

PFS will perform measurement when the spacecraft is below 4000 km. PFS will wake up from its sleep mode about 1 h before and follow the scheme:

- apocentre: PFS is in sleep mode, telecommands can be received;
- pericentre minus 60 min: wake-up, wait for warm-up, start autonomous test, calibration LW, calibration SW, calibration deep space. PFS-S in nadir direction. Give data to the spacecraft;
- pericentre minus 40 min: start martian observations. Give data to the spacecraft;
- pericentre plus 48 min: stop martian observations. Give data to the spacecraft;
- pericentre plus 53 min: calibration LW, calibration SW, calibration deep space, autonomous test. Give data to the spacecraft. Go into sleep mode;
- up to apocentre in sleep mode.

In total, 600 measurements per orbit are taken, of which 60 are calibrations. This corresponds to 1200 measurements per day (the third orbit per day being for downlink) and 823 440 spectra in a martian year. The footprint from 4000 km is of the order of 109 km for the SW channel and 188 km for the LW channel; at pericentre (250 km) they become respectively 6.8 km and 11.8 km (perpendicular to the ground track, but 20 km along it) .

References

Arnold, G., Hirsch, H., Formisano, V. & Moroz, V. (1993). Studies of Martian Atmosphere and Surface by the Planetary Fourier Spectrometer on Board of the Mars-94 Mission. *Proc. SPIE 2089*, 284.

Atreya, S.K. (1989). The Martian Upper Atmosphere. In *Colloque International, Premiere Resultats de la Mission Phobos et Future Missions d'exploration de Mars*, CNES, Paris, France, p42.

Bartholomew, M.J., Cruikshank, D.P. & Roush, T. (1990). Asteroid and Meteorite Spectral Analogs for Phobos. *Bull. Amer. Astro.Soc.* **22**, 1115.

Carr, M.H. (1974). The Geology of Mars. In *A Primer in Lunar Geology*, NASA Ames Research Center, pp459-460.

Haberle, R.M. (1986). The Climate of Mars. *Sci. Am.* **254**, 54-62.

Haberle, R.M. & Jakowsky, B.M. (1990). Sublimation and Transport of Water from the North Residual Polar Cap on Mars. *J. Geophys. Res.* **95**, 1423.

Hanel, R.A., Conrath, B.J., Jennings, D.E. & Samuelson, R.E. (1992). *Exploration of the Solar System by Infrared Remote Sensing*, Cambridge University Press, UK.

Hanel, R., Conrath, B., Howis, W., Kunde, V., Lowman, P., Maguire., W., Pearl, J., Pirraglia, J., Prabhakara, C. & Schlachman, B. (1972). Investigation of the Martian Environment by Infrared Spectroscopy on Mariner-9. *Icarus* **17**, 423-442.

Hansen, G.B. (1997). The Infrared Absorption Spectrum of Carbon Dioxide Ice from 1.8 to 333 µm. *J. Geophys. Res.* **102**, E9, 21569-21588.

Hirsch, H. & Arnold, G. (1993). Fourier Transform Spectroscopy in Remote Sensing of Solid Planetary Surfaces. *Vib. Spectrosc.* **5**, 119-123.

Hirsch, H. (1997). Optical Design and Performance of the Planetary Fourier Spectrometer (PFS). *Mcrochimica Acta [Suppl.]* **14**, 571-574.

Hunt, G.R., Logan, L.M. & Salisbury, J.W. (1973). Mars: Components of Infrared Spectra and Composition of the Dust Clouds. *Icarus* **18**, 459.

Hunt, G.R., Salisbury, J.W. & Lenhoff, C.J. (1974).Visible and Near Infrared Spectra of Minerals and Rocks: IX. Basic and Ultrabasic Igneous Rocks. *Modern Geology* **5**, 15-22.

Jakosky, B.M. & Haberle, R.M. (1992). The Seasonal Behavior of Water on Mars. In *Mars* (Eds. H.H. Kieffer, B.M. Jakosky, C.W. Snyder & M.S. Matthews), The University of Arizona Press, Tucson, USA, pp969-1016.

Jakosky, B.M. & Farmer, C.B. (1982). The Seasonal and Global Behavior of Water Vapor in the Mars Atmosphere – Complete Global Results of the Viking Atmospheric Water Detector Experiment. *J. Geoph. Res.* **87**, 2999-3019.

Justus, C.G., James, O. & Johnson, A. (1995). *Mars Global Reference Atmospheric Model (Mars-GRAM 3.34): Programmer's Guide*. Computer Sciences Corp., USA.

Kahn, R.A., Martin, T.Z., Zurek, R.W. & Lee, S.W. (1992). The Martian Dust Cycle. In *Mars* (Eds. H.H. Kieffer, B.M. Jakosky, C.W. Snyder & M.S. Matthews), The University of Arizona Press, Tucson, USA, pp1017-1053.

Kaplan, L.D., Munch, G. & Spinrad, H. (1964). An Analysis of the Spectrum of Mars. *Astrophys. J.* **139**, 1.

Kieffer, H.H., Martin, T.Z., Peterfreund, A.R., Jakosky, B.M., Miner, E.D. & Palluconi, F.D. (1977). Thermal and Albedo Mapping of Mars during the Viking Primary Mission. *J. Geoph. Res.* **82**, 4249-4291.

Kliore, A.J., Cain, D.L., Fjeldbo, G., Seidel, B.L., Sykes, M.J. & Rasool, S.I. (1972). The Atmosphere of Mars from Mariner 9 Radio Occultation Measurements. *Icarus* **17**, 484-516.

Kliore, A.J., Woiceshyn, P.M. & Hubbard, W.B. (1977). Pioneer 10 and 11 Radio Occultations by Jupiter. In *Symposium on Minor Constituents and Excited Species*, Philadelphia, Pa., USA, 9-10 June 1976 (A78-18101 05-42), p703-710.

McCord, T.B. & Cruikshank, D.P. (1981). Spectrophotometric Remote Sensing of Planets and Satellites. In *Infrared Astronomy; Proceedings of the Symposium*, Kona, HI, USA, 23-27 June 1980 (A82-33729 16-90), p57-87.

Morris, R.V. & Lauer, H.V. (1990). Matrix Effects for Reflectivity Spectra of

Dispersed Nanophase (Usuperparamagnetic) Hematite with Application to Martian Spectral Data. *J. Geophys. Res.* **95**, 5101.

Moroz, V. & Nadzhip, A.E. (1975). Measurements of Water Vapour Densities on Mars 5 Orbiter: Preliminary Results. *Cosmic Res.* **13**, 28.

Owen, T. (1992). The Composition and Early History of the Atmosphere of Mars. In *Mars* (Eds. H.H. Kieffer, B.M. Jakosky, C.W. Snyder & M.S. Matthews), The University of Arizona Press, Tucson, USA, pp818-834.

Owen, T., Maillard, J.P., de Bergh, C. & Lutz, B.L. (1988). Deuterium on Mars: The Abundance of HDO and the Value of D/H. *Science* **240**, 1767.

Pedlosky, J. (1979). *Geophysical Fluid Dynamics*, Springer-Verlag, Germany.

Pollack, J.B. & Toon, O.B. (1982). Quasi Periodic Climate Changes on Mars: A Review. *Icarus* **50**, 259.

Pollack, J., Roush, T., Witteborn, F., Bregman, J., Wooden, D., Stoker, C., Toon, O., Rank, D., Dalton, B. & Freedman, R. (1989). Thermal Emission Spectra of Mars (5.4-10.5 mm): Evidence for Sulfates, Carbonates and Hydrates. In *Colloque International, Premiere Resultats de la Mission Phobos et Future Missions d'exploration de Mars*, CNES, Paris, France, p93.

Pollack, J.B., Colburn, D.S., Flasar, F.M., Kahn, R., Carlston, C.E. & Pidek, D.G. (1979). Properties and Effects of Dust Particles Suspended in the Martian Atmosphere. *J. Geoph. Res.* **84**, 2929-2945.

Rieder, R., Wänke, H., Economou, T. & Turkevich, A. (1997). Determination of the Chemical Composition of Martian Soil and Rocks: The Alpha Proton X-ray Spectrometer. *J. Geoph. Res.* **102**, E2, 4027-4044.

Rodin, A.V., Korablev, O.I. & Moroz, V.I. (1997). Vertical Distribution of Water in the Near-Equatorial Troposphere of Mars: Water Vapor and Clouds. *Icarus* **125**, N1, 212-229.

Rothman, L.S., Gamache, R.R., Tipping, R.H., Rinsland, C.P., Smith, M.A.H., Benner, D.C., Devi, V.M., Flaud, J.-M., Camy-Peyret, C. & Perrin, A. (1992). The HITRAN Molecular Data Base – Editions of 1991 and 1992. *J. Quan. Spect. & Rad. Transfer* **48**, N5-6, 469-507.

Roush, T.L., Blaney, D.L. & Singer, R.B. (1993). The Surface Composition of Mars as Inferred from Spectroscopic Observations. In *Remote Geochemical Analysis: Elemental and Mineralogical Composition*, (Eds. C.M. Pieters & P.A.J. Englert), Cambridge Univ. Press, UK, pp367-393.

Roush, T.L., Pollack, J.B., Stoker, C., Witteborn, F., Bregman, J., Wooden, D. & Rank, D. (1989). CO^{32} and SO^{42-}-bearing Anionic Complexes Detected in Martian Atmospheric Dust. *Lunar Planet. Sci. Conf. XX*, p928.

Seiff, A. (1982). Post-Viking Models for the Structure of the Summer Atmosphere of Mars. *Adv. Space Res.*, **2**, N2, 3-17.

Smith, W.L. (1970). Iterative Solution of the Radiative Transfer Equation for the Temperature and Absorbing Gas Profile. *Appl. Optics* **9**, N9,1993-1999.

Soderblom, L.A. (1992). The Composition and Mineralogy of the Martian Surface from Spectroscopic Observations: 0.3 mm to 50 mm. In *Mars* (Eds. H.H. Kieffer, B.M. Jakosky, C.W. Snyder & M.S. Matthews), The University of Arizona Press, Tucson, USA, pp557-593.

Spinrad, H. & Richardson, E.H. (1963). High Dispersion Spectra of the Outer Planets. II. A New Upper Limit for the Water Vapor Content of the Martian Atmosphere. *Icarus* **2**, 49.

Tikhonov, A.N., Goncharskij, A.V., Stepanov, V.V. & Jagola, A.G. (1990). *Numerical Methods of Solving the Ill-posed Problems.* Nauka, Moscow (in Russian).

Toulmin, P., Baird, A.K., Clark, B.C., Keil, K., Rose, H.J., Christian, R.P., Evans, P.H. & Kelliher, W.C. (1977). Geochemical and Mineralogical Interpretation of the Viking Inorganic Chemical Results. *J. Geophys. Res.* **82**.

Zurek, W.R., Barnes, J.R., Haberle, R.M., Pollack, J.B., Tillman, J.E. & Leovy, C.V. (1992). Dynamics of the Atmosphere of Mars. In *Mars* (Eds. H.H. Kieffer, B.M. Jakosky, C.W. Snyder & M.S. Matthews), The University of Arizona Press, Tucson, USA, pp799-817.